Shape characteristics of freshly fallen snowflakes and their short-term changes

S. R. FASSNACHT, E. D. SOULIS & N. KOUWEN
Department of Civil Engineering, University of Waterloo, Waterloo, Ontario, Canada N2L 3G1
e-mail: srfassna@uwaterloo.ca

Abstract The shape of newly formed snowflakes is an important qualitative parameter as input to the development of a snowpack, and for potential atmospheric scavenging, while changes in the shape of freshly fallen crystals influence the metamorphosis and transport of snow and contaminants. This paper uses known spatial properties to simulate the needle-shaped crystal structures that can occur in the range of –4 to –6°C. Probability distribution functions (pdfs) are derived for the surface area to mass ratio, ranging from 0.10 to 0.30 $m^2 g^{-1}$. Observations of freshly fallen flakes are compared to predicted pdfs. The modification in the snow crystal shape, immediately after accumulation, is estimated from laboratory experiments that measured sublimation rates directly from the pack. For fresh flakes, there is a rapid decrease in the effective surface area up to 50% over only 2–3 days.

INTRODUCTION

Knowledge of the shape and history of falling snowflakes is important to assess the metamorphosis and evolution of an accumulating snowpack layer, and the potential atmospheric scavenging that can occur during descent. Changes in the shape of crystals at the top of a snowpack influence the transport potential for blowing snow, the direct sublimation rate, as well as the immediate fate of contaminants within crystals and through the pack. Few methods exist to estimate either the initial shape or subsequent change.

Various investigations have examined the surface area of ice crystals, particularly for the adsorption of nitrogen at low temperatures in the range of –195°C (e.g. Adamson & Dormant, 1966; Ghormley, 1967), resulting in estimates of ice surface areas from 200 to 500 $m^2 g^{-1}$. However few of these experiments used actual snow at expected outdoor temperatures, i.e. –20°C or warmer. Adamson & Dormant (1966) measured the surface area to mass ratio or specific surface area (SSA) of two falling snow samples to be 0.2 and 0.4 $m^2 g^{-1}$, although they considered these to be very low due possibly to the adsorption of atmospheric impurities. Hoff *et al.* (1998a) used Nitrogen Adsorption specifically to measure the SSA of fresh snow samples and yielded a range from 0.06 to 0.37 $m^2 g^{-1}$. Hoff *et al.* (1998b) also summarized various results of using light and scanning electron microscopes to view snow crystals and estimated a snow SSA range from 0.05 to 0.5 $m^2 g^{-1}$, with a likely maximum of 1.0 $m^2 g^{-1}$.

In preliminary results, Hoff *et al.* (1998b) presented data illustrating a decrease in SSA of 40% in less than 2 days for one snowpack sample and in 4.5 days for the second sample. Jellinek & Ibrahim (1967) proposed an empirical model to quantify the SSA decrease rate for artificial ice powders. They stated that a first-order law can represent the first 40% decrease in surface area, after which the rate of SSA decrease slows until no further SSA reduction at a 60% decrease (Jellinek & Ibrahim, 1967). Hoff *et al.* (1998b) calculated a half-life for the SSA of fresh snow to be either 46 h (from Jellinek & Ibrahim, 1967), or 33 h (from Wania, 1997).

The objectives of this paper are as follows: to present a method of estimating the surface area to mass ratio of fresh snowflakes, in particular needle shaped crystals that form between –4°C and –6°C; and to illustrate the rapid decrease in specific surface area of crystals within a snowpack, derived from the difference of laboratory measurements of sublimation and computed estimates. While the SSA is modelled for individual crystals and the experimental measurements consider SSA decreases of the snowpack, these two different techniques both emphasize the estimation of snow crystal characteristics.

NUMERICAL THEORY

Particle relationships

Snow crystals form as small hexagonal plates that can grow along the six prism faces (*a*-axis) and/or perpendicularly along the two basal planes (*c*-axis).In summarizing previous work, Ono (1970) described the change of the ice crystal form with temperature. Column and needle shaped crystals grow primarily along the *c*-axis, while plate and stellar dendrites grow primarily along the *a*-axis. This paper focuses on needle shaped columnar crystals that form between –4°C and –6°C and growth is confined to the *c*-axis.

Ono (1970) graphically presented relationships between the lengths (*c*-axis) and widths (*a*-axis) of crystals for different columnar forms (–3.5 to –9.5°C), and the growth mode at different temperatures. The dimensions of most snow crystal types were analysed by Auer & Veal (1970) to produce empirical relationships over a large range of sizes. The following relationship describes the length (L)–width (W) relationship for needle crystals:

$$W = 1.099 L^{0.61078} \tag{1}$$

for lengths from 16 to 2800 μm (Auer & Veal, 1970). In comparing the width to height for needles, Auer & Veal's (1970) conclusion that the crystals are cylindrical agrees with the investigations by Nakaya (1954) and Magono & Lee (1966). The measurements of width and length by Hobbs *et al.* (1974) yielded an empirical relationship of a different form:

$$\ln W = -10.76 + 4.159 \ln L - 0.2882 (\ln L)^2 \tag{2}$$

for a range of lengths from 200 to 1500 μm. Equations (1) and (2) produce similar curves that fit the data of previous researchers well.

Sublimation

To determine the changes in the SSA of the snowpack, the measured sublimation is compared to computed sublimation. The mass and heat transfer equations that govern sublimation express the latent heat required for phase change and the energy available from the environment in terms of sensible heat. Sverdrup (1936) derived equations for air movement over snow by considering eddy conductivity. The amount of water transported away from or towards the surface was defined as a function of the eddy conductivity and the change in the specific humidity of air (q) with respect to the height above the surface (z).This mass transport (F with units of mass per time per area) explaining the vertical distribution and exchange of water vapour was given as:

$$F = \rho_a k_o^2 \frac{U_a}{\ln\left(\frac{a+z_d}{z_o}\right)} \frac{q_b - q_o}{\ln\left(\frac{b+z_d}{z_o}\right)} \tag{3}$$

where ρ_a is the density of water vapour, k_o is the von Karman roughness coefficient, U_a is the wind velocity at height a, z_o is the roughness height, z_d is the zero-plane displacement, b is the measurement height of q, and q_o is the specific humidity at the surface of the snow. The heat transported towards the surface (Q as energy per unit time per area) is a function of the specific heat capacity of air (c_p), the eddy conductivity under stable air, and the change in the potential temperature of air (θ) with respect to the height above the surface. It is defined as:

$$Q = c_p \rho_a k_o^2 \frac{U_a}{\ln\left(\frac{a+z_d}{z_o}\right)} \frac{\theta_b - \theta_o}{\ln\left(\frac{b+z_d}{z_o}\right)} \tag{4}$$

where the potential temperature (θ_b) is measured at height b. This potential temperature considers the vertical atmospheric stability in terms of pressure change from the surface to the measurement height.

Light (1941) assumed no zero-plane displacement, and measurement of all environmental parameters at the same height above the surface (a).The mass transfer equation (1) was rewritten as a function of vapour pressures at height (e_b) and at the surface (e_o), and air pressure (p) as follows:

$$F = \frac{0.623}{p} \frac{\rho_a k_o^2}{[\ln(a/z_o)]^2} U_a (e_a - e_o) \tag{5}$$

The lapse rate was assumed to be minimal for typical measurement heights, i.e. there was no significant atmospheric pressure change. Therefore the heat transfer equation (2) could be expressed as a function of the difference between the air temperature (T_a) at height a and the surface temperature (T_o) as follows:

$$Q = c_p \frac{\rho_a k_o^2}{[\ln(a/z_o)]^2} U_a (T_a - T_o) \tag{6}$$

The sublimation rate is dictated by the limiting quantity of energy available (described in equation (4)), and energy required based on the vapour pressure gradient (equation

(3) multiplied by the latent heat of sublimation). However, these two quantities are not independent; the ambient vapour pressure, and hence the vapour pressure deficit, reflects the temperature, which adjusts to the available energy. Thus for steady-state conditions, the available and required energy reach an equilibrium.

METHODOLOGY

Particle surface area

Since it is a common belief that no two snowflakes are alike, a Monte Carlo simulation will be used to estimate the specific surface area of needle-shaped snow crystals. Based on personal observations of needles, as well as pictures in the literature, a general shape can be assumed (see Fig. 1). Such a needle is cylindrical with indented or cupped ends. It is partially hollow between the cupped ends when the needle width is significantly larger than its thickness (making it sheath-like). The ends of the needle are usually jagged, yet the surface area within the cupped ends is much greater than variation due to jaggedness of the ends. However, to consider the uneven ends, the surface area of the ends is doubled.

Auer & Veal (1970) and Hobbs *et al.* (1974) both give ranges of observed crystal lengths, however no distributions have been found in the literature for the probability distribution function (pdf) of needle crystals. Although the data collected by Grunow & Huefner (1959) are limited to plate shapes, it is assumed that the distribution for stellar crystals is similar to that of needles since both grow primarily along one axis at a maximum rate (as illustrated by Ono, 1970). Since the growth rate of stellars is greater than that of needles, and personal observation has shown that stellars are typically larger, the shape of the stellar pdf presented by Grunow & Huefner (1959) will be used, but shifted. Figure 2 illustrates the transformed data with a uniform pdf defined by the applicability range of the Hobbs *et al.* (1974) relationship, and a lognormal pdf. The width, sheath thickness, and depth of cupping will all assume normal pdfs.

For each simulated crystal, the length will be randomly chosen (from within the desired pdf) and the corresponding mean width will be calculated using the Auer & Veal relationship. The standard deviation is assumed to be one-sixth of the mean. The walls of the needle have been assigned a mean thickness of 10 μm based on the minimum diameter required to sustain existence (i.e. to not evaporate) and crystal observations such as Rango *et al.* (1996). The standard deviation of thickness is assumed to be 1.25 μm. The depth of each indentation into the ends of the needle is assumed to be a function of the total crystal length with a mean of 10% and a standard

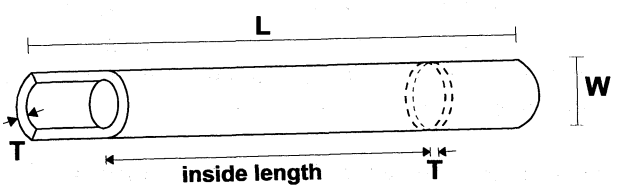

Fig. 1 Schematic of the needle shaped crystal used in the numerical simulations.

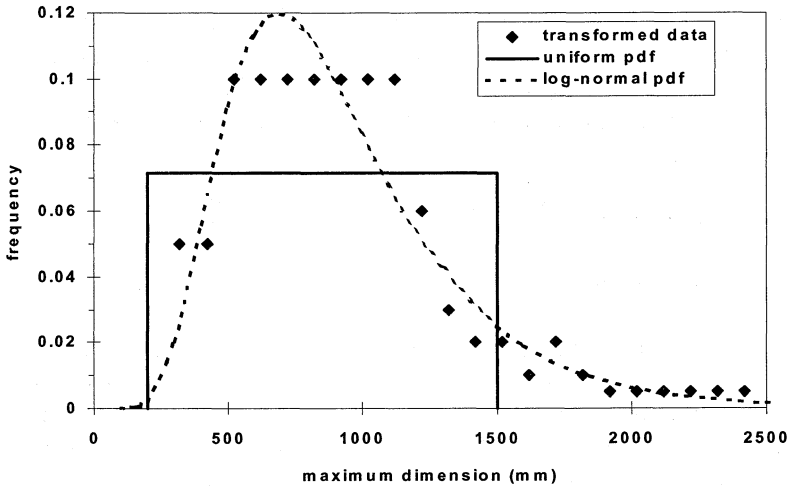

Fig. 2 Probability distributions for the maximum dimension of needle crystals transformed from stellar crystal data from Grunow & Huefner (1959).

deviation of 1.25%, for each end. Using a density of ice of 0.915 g m^{-3}, the surface area to mass ratio can then be determined by the randomly selected dimensions for the unrimed needle-shaped crystal.

Riming is accretion of small particles that freeze onto the surface of snow crystals falling through a cloud of supercooled water droplets. Due to the small nature of rime particles, it could be assumed that the rime particles form frozen hemispheres or grow into mini-hexagonal crystals. However, Rango *et al.* (1996) illustrated the accumulation of rime along one edge of a hexagonal plate and stated that the rime particles appear to be needles, 5 μm in diameter and 20 μm in length. The degree of riming is difficult to assess since it depends upon conditions through which the crystals fall. Therefore, crystals will be simulated with no riming, 20% riming, and 50% riming. The riming will be assumed to occur only the outer surface and not within the cupped ends.

Surface area changes

The sublimation process is influenced by atmospheric variables and snow particle characteristics (size, shape, etc.). However, the mass and heat transfer expressions described above (equations 3 and 4) do not consider the influence of snow particle size or shape. For the sublimation from particles during blowing snow, instead of directly from the pack, Thorpe & Mason (1966) examined non-spherical crystals and introduced a shape factor for plate-type snow crystals. However, if all the sublimation losses in the experiments are directly from the snow surface and not particle transport, the difference between the observed sublimation and the estimated sublimation may be indicative of intricate surface shapes.

Laboratory experiments The experiments were performed in a cold room operated by the Department of Civil Engineering at the University of Waterloo. The

cold room has a volume of approximately 4 m^3 and is insulated by 8 cm foam within steel walls plus 5 cm Styrofoam insulation. The temperature is maintained in the chamber by an internal compressor unit that ran on a 24 h defrost cycle. To reduce the humidity and temperature variation of the experiment, the experimental area was isolated from the compressor unit by a double sheet of 5 mil polyethylene plastic. The sublimation apparatus was housed in a box sealed by polyethylene plastic except for the entrance fan and an exit port.

The experimental area within the cold room can be assumed to be a sealed box with respect to vapour movement. This box has an input of heat through the walls driven by the temperature gradient between the external building air (in the range of 18 to 25°C) and the air inside the cold room (internally less than –1°C). This heat is removed from the box by the compressor unit. The placement of exposed snow samples in the box provides an additional heat sink to remove some energy input as longwave radiation, conducted heat and vapour momentum.

Apparatus Undisturbed snow was placed in a small evaporation pan with a diameter of 61 cm (2 feet) and a depth of 12.7 cm (5 inches) that was constructed from galvanized steel. The pan was mounted on three knife-blade edges at the ends of 2.5-cm box beams. The three box beams were attached together at the opposite ends, below the centre of the pan, by a bolt into load cell, and were supported by three knife-blade edges. These knife blades sat on a three arm base built of 12.7 cm I-beams. Each I-beam was welded to the adjacent beam 25 cm from the end to create an empty triangular space, 20 cm in length. A 1.5 cm piece of steel was welded to the underside of each I-beam flange to create a triangular support at the centre of the I-beam base that held the bottom of the 12 kg (25 lb) S-shaped load cell (manufactured by ARTECH Industries). The load cell measured changes in load in terms of voltage. Upon calibration, the data acquisition unit recorded mass in kilograms with a precision of ±7 g. The deformation of the apparatus and pan were assumed to be minimal since the sublimation losses were measured as a function of the initial snow plus apparatus mass, and total the mass usually decreased by less than 20% over each experimental run. The initial mass was taken as the average mass of the first 20 readings to decrease the effect of voltage fluctuation through the load cell.

The temperature was measured near the surface of the snowpack using a thermocouple, and at the side of the basket and a metre away using voltage (a VAISALLA converting 0 to 5 V to –20°C to +80°C) to represent ambient air temperature. The relative humidity was determined at the side of the basket and a metre away using the difference between dry and wet bulb temperatures. The basket load, temperatures, and relative humidity were recorded every three minutes based on the continuous average value sampled for each parameter over the three-minute period.

The ventilation wind was achieved using a 25 cm fan. As the wind speed varied at the snowpack surface with time due to the placement of the fan at one end of the basket and to the depletion of the snow, the wind speed was measured across the pan at several heights throughout each experiment. A digital display hot-wire anemometer (KANOMAX Climomaster 6511 with a flexible tip) was used to measure the point wind speeds, and the mean velocities were calculated by determining the volume under the velocity surface derived from kriging the point measurements.

Surface area change calculations During each experimental run, environmental conditions and loads were measured every three minutes. These data were averaged to provide 12-h estimates of sublimation losses, and environmental parameters for two different sensors (labelled 1 and 2). These parameters were used with equations (3) and (4) to calculate four different expected sublimation losses. For the heat and mass transfer estimates of sublimation, a roughness height of 0.5 cm was calculated using a relationship developed by Lettau (1969), and the von Karman constant was assigned a value of 0.40 (from Oke, 1987). The percent mass loss difference between the observed and computed sublimation losses was then calculated based on the two methods for the two sensors.

RESULTS AND DISCUSSION

Surface area of needle-shaped crystals

The non-rimed needle-shaped crystal probability distributions using the uniform and lognormal length distributions are very similar, with mean for the non-riming scenarios of 0.157 and 0.154 $m^2 g^{-1}$, respectively (Fig. 3). For 20% riming with the two different pdfs, the average and range of surface areas are also similar. However the cylindrical (needle) rime increases the surface area by 27%, from 0.167 to 0.213 $m^2 g^{-1}$, over the hemispherical rime. For a rime coverage of 50%, the surface area increases by 53% (from 0.183 to 0.280 $m^2 g^{-1}$). The surface area increase per % riming was approximately 0.0006 $m^2 g^{-1}$ $\%rime^{-1}$ for the hemispherical rime droplets and approximately 0.0030 $m^2 g^{-1}$ $\%rime^{-1}$ for the needle shaped rime, observed by Rango *et al.* (1996). As can be expected the SSA increase per % riming decreases as the crystal becomes more rime covered. At 10% needle rime cover, the SSA increases by

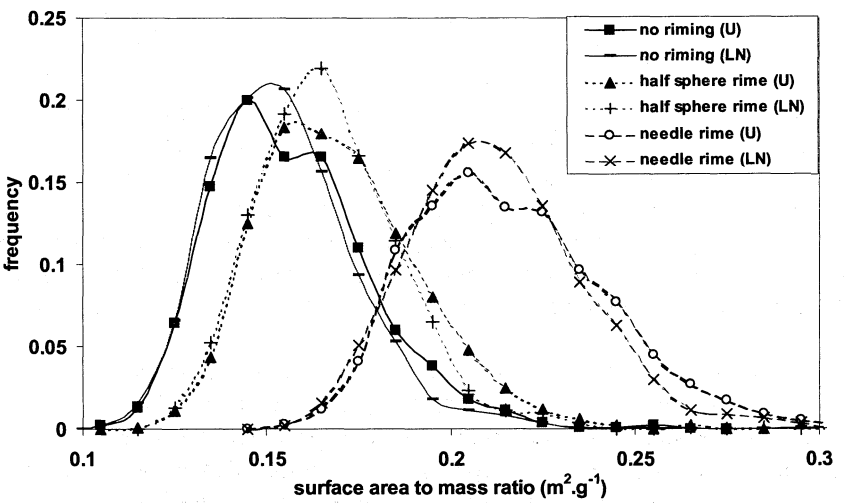

Fig. 3 Probability distributions for non-rimed and 20% rimed needle crystals, assuming half-sphere rime and needle-rime, using a uniform and log-normal pdf for the length distribution.

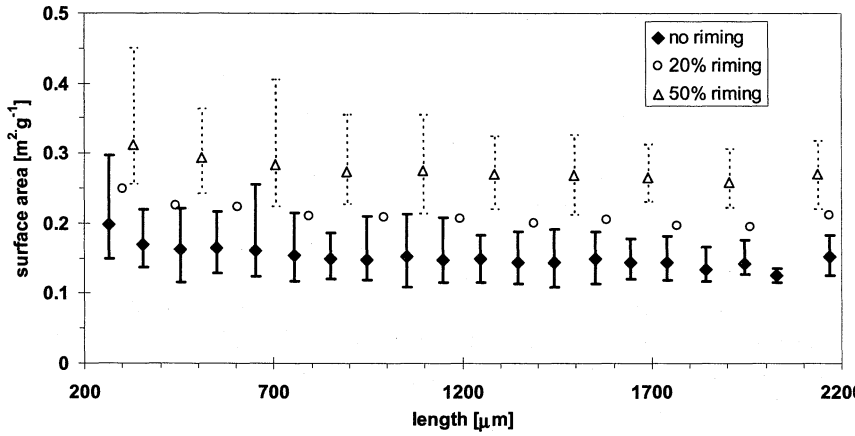

Fig. 4 Average, maximum and minimum surface area for non-rimed, 20% rimed, and 50% rimed. Riming assumes needle-shaped rime and length uses a log-normal pdf.

2% per % rime (0.42% per % rime for hemispherical rime), whereas at 80% the increase is 1.44% per % rime (0.33% per % rime for hemispherical rime).

The surface area decreases as the length of the crystal increases (see Fig. 4). This agrees with the power-law calculations by Hogan (1994) for various crystal types across a size distribution of 1.4 standard deviations. Although Hogan did not calculate the area to mass ratio for needles, the results from this research fit into the range of thin plates (Magono and Lee crystal type P1d). While the surface area increases as riming increases, the decrease in mean surface area with increased length is approximately the same for non-rimed and rimed conditions, i.e. the slope of the average surface area remains constant regardless of riming.

The surface areas simulated in this research fall within the range of measurements by Hoff *et al.* (1998a). Unlike Hoff *et al.* (1998a), this paper looks at a specific crystal type and the simulation of crystal geometry, which has the potential to provide surface area detail that can be linked to temperature. Thus, with further work air temperatures may provide rough estimates of the surface area of falling snow.

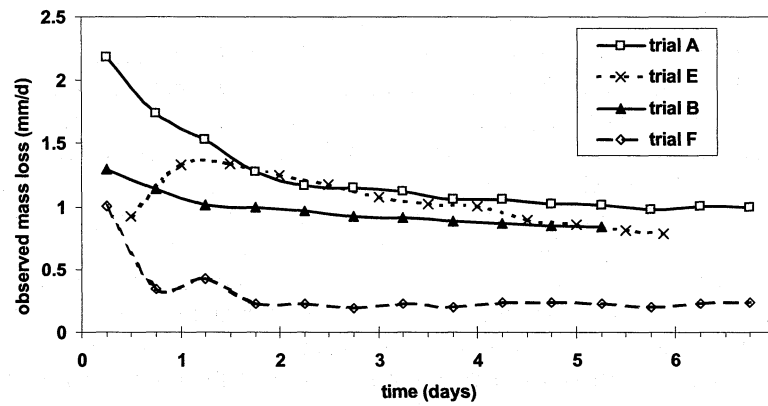

Fig. 5 Observed 12-h average sublimation losses (in millimetres per day) for four different experimental trials.

Sublimation measurement of surface area changes

The sublimation that was measured in the laboratory was directly from the snowpack samples, and there was no transport of snow crystals. Li & Pomeroy (1997) show that the threshold wind speed for movement of snow particles at a measurement height of 10 m is usually greater than 5 m s^{-1}, but with few instances as low as 4 m s^{-1}. Using the logarithmic wind profile equation (Oke, 1987), the maximum 10-m wind speed for the experiments A, B, E, and F was 3.2, 3.4, 1.3 and 0.85 m s^{-1}, respectively. Therefore none of the crystals were blown from the sublimation pan.

The laboratory sublimation rates after 2 days started to approach steady-state values (see Fig. 5) in the order of 1 mm day^{-1} for trials A, B and E, and 0.3 mm day^{-1} for trial F. These are well within the rates observed in field experiments. For example, Williams (1959) observed rates between 0.029 and 1.642 mm day^{-1} and Martinelli (1960) observed losses between 0.668 and 1.219 mm day^{-1}.

The difference between the observed and computed mass loss through sublimation using the two sensors and two methods (heat and mass transfer) for experiment "A" are presented in Fig. 6. The heat and mass transfer approaches yield almost the same percent differences after the first day, whereas there is more than a 50% difference between the mass and heat transfer results from sensor 2 calculations until day 5. Since this trend was present for all other experiments, the expected differences between observed and computed mass losses are computed by the heat transfer approach and first-order law curves are fitted to these data (see Fig. 7). The curves fit the data well with r^2 values of 0.989, 0.935, 0.804 and 0.883, for experiments A, B, E and F, respectively. The half-life for snow surface area was calculated to be 25 and 59 h for experiments A and B, which is in the same range as the half-life calculated by Wania (1997) of 33 h and Jellinek & Ibrahim (1967) of 46 h. As illustrated in Fig. 7, the half-life of the snow surface area for experiment E and F are much smaller (2 h) and much greater (142 h), respectively, yet both experiments do illustrate the probable decrease in surface area over time.

Sublimation is not just from the surface of the pack. Since snow is a porous media, wind can penetrate into the pack allowing a vapour pressure deficit to exist at depth. The movement of air through the snowpack samples is likely along the surface and through the first centimetre of depth, or more (even with no surface undulations). While sublimation is causing a mass loss at the surface, lower particles will undergo a shape change. This is a sublimation–resublimation process that reshapes the snow crystals due to the surface energy differences between protruding areas with large curvature and indentations. The redistribution of molecules may be dominated by a non-reversing solid to vapour phase change resulting in a net mass loss (Calvert & Brock, 1972), but more importantly it is a reshaping from irregular towards a regular, almost spherical shape. Also the weight of overlying particles causes a mechanical breakage of the same areas that undergo shape change first, i.e. crystals with high curvature and hence larger surface areas. Thus the metamorphosis of snow crystals decreases the exposed surface area of snow crystals and can explain most of the decrease in the sublimation rate with time. During examination of snow crystals using a microscope, Nakaya (1954) recognized the importance of sublimation. Particularly for dendritic crystals, there is a size decrease and a loss of the finer patterns, similar to a smudging or smearing effect (Nakaya, 1954).

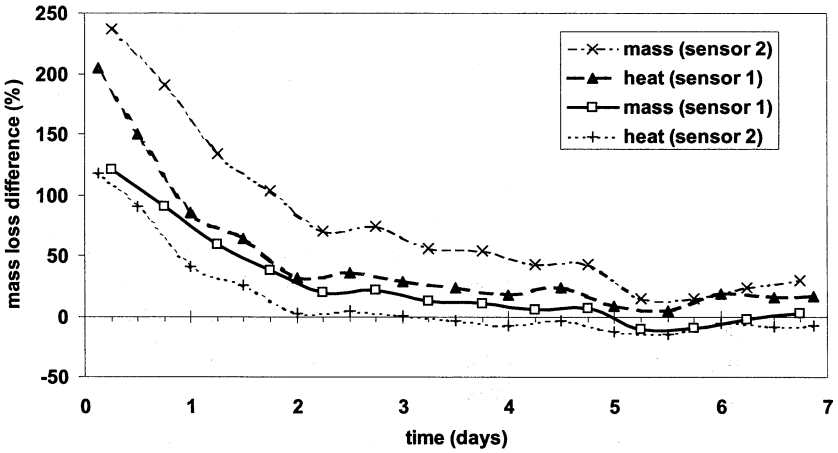

Fig. 6 Percent mass loss difference between observed and computed sublimation using mass and heat transfer formulae for two different sensors for experiment "A".

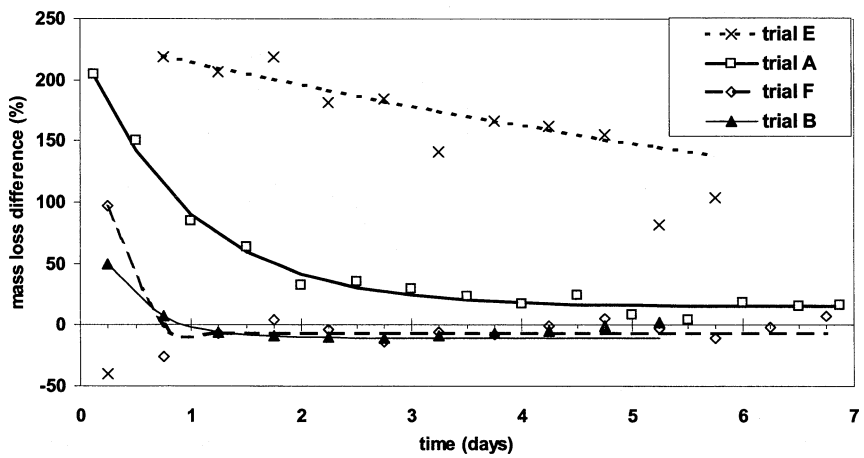

Fig. 7 Plot of percent mass loss difference between the observed and computed (heat transfer method using sensor #1 data) sublimation and fitted decay curves for the four experiments.

For fresh snow, sublimation rates may vary with size and type of crystal. Since flake types are a function of formation conditions, in particular, temperature, it may be possible to use weather conditions to classify the cover of the pack according to flake type. However, the age of snow is also an important parameter influencing sublimation. The age of the snow can be used to estimate a snow "history" of exposure conditions, as well as the rate of change in the exposed surface area of the snow.

CONCLUSIONS

A method was presented to estimate the surface area to mass ratio of needle shaped

ranged from 0.1 to 0.3 $m^2 g^{-1}$, with a mean of 0.15 $m^2 g^{-1}$. Riming can increase the specific surface area by up to 2% per % rime cover for needle shaped rime, resulting in an increase in the surface area range to between 0.21 and 0.45 $m^2 g^{-1}$ for 50% coverage, with a mean of 0.28 $m^2 g^{-1}$.

The use of known particle relationships to simulate crystals provides decent surface area estimates for needle shaped crystals. This method should be expanded with the assistance of scanning electron microscope images and nitrogen adsorption measurements to examine the surface areas of various crystal types that form at different temperatures. The shape of rime particles and degree of riming with respect to different snow crystal shapes should be further investigated to better assess the surface area differences caused by riming.

While the experimental measurements did not directly measure the specific surface area decreases of a snowpack over time, these changes were inferred from the difference of laboratory measurements of sublimation and computed estimates.

Acknowledgement The financial support provided by Atmospheric Environment Service of Environment Canada through the CRYSYS project and science subventions is gratefully acknowledged. Discussions with Dr J. Pomeroy of NHRI provided invaluable insight into the complex process of sublimation.

REFERENCES

Adamson, A. W. & Dormant, L. M. (1966) Adsorption of nitrogen on ice at 78 K. *J. Am. Chem. Soc.* **88**(9), 2055–2057.

Auer, A. H., Jr & Veal, D. L. (1970) The dimensions of ice crystals in natural clouds. *J. Atmos. Sci.* **27**, 919–926.

Calvert, B. & Brock, D. (1972) Silver machine. Part 6 in: *Psychedelic Warlords*, reissue 1996. Cleopatra, Los Angeles, California.

Ghormley, J. A. (1967) Adsorption and occlusion of gases by low temperature forms of ice. *J. Chem. Phys.* **46**(4), 1321–1325.

Grunow, J. & Huefner, D. (1959)Observations and analysis of snow crystals for proving the suitability as aerological sonde. Final Report USA Contract DA 91 508 EUC 285, Hohenpeissenberg, Oberbayern AD 217431.

Hobbs, P. V., Chang, S. & Locatelli, J. D. (1974) The dimensions and aggregation of ice crystals in natural clouds. *J. Geophys. Res.* **79**(15), 2199–2206.

Hoff, J. T., Gregor, D., Mackay, D., Wania, F. & Jia, C. Q. (1998a) Measurement of the specific area of snow with the nitrogen adsorption technique. *Environ. Sci. Technol.* **32**(1), 58–62.

Hoff, J. T., Wania, F., Mackay, D., Semkin, R. & Jia, C. Q. (1998b) Quantifying the atmospheric delivery of organic contaminants into the high arctic marine ecosystem as influenced by snow and ice. Progress Report to the Department of Indian and Northern Affairs, Canada.

Hogan, A. W. (1994) Objective estimates of airborne snow properties. *J. Atmos. Oceanic Tech.* **11**, 432–444.

Jellinek, H. H. G. & Ibrahim, S. H. (1967) Sintering of powdered ice. *J. Colloid Interface Sci.* **25**, 245–254.

Lettau, H. (1969) Note on aerodynamic roughness-parameter estimation on the basis of roughness-element description. *J. Appl. Met.* **8**(5), 828–832.

Li, L. & Pomeroy, J. W. (1997) Estimates of threshold wind speeds for snow transport using meteorological data. *J. Appl. Met.* **36**, 205–213.

Light, P. (1941) Analysis of high rates of snow-melting. *Trans. Am. Geophys. Un.*, 195–205.

Magono, C. & Lee, C. W. (1966) Meteorological classification of natural snow crystals. *J. Fac. Sci. Hokkaido Univ.*, series 7(II), 321–335.

Martinelli, M., Jr (1960) Moisture exchange between the atmosphere and alpine snow surfaces under summer conditions (preliminary results). *J. Met.* **17**, 227–231.

Nakaya, U. (1954) *Snow Crystals: Natural and Artificial.* Harvard University Press.

Oke, T. R. (1987) *Boundary Layer Climate*, 2nd edn. Routledge.

Ono, A. (1970) Growth mode of ice crystals in natural clouds. *J. Atmos. Sci.* **27**, 649–658.

Rango, A., Wergin, W. P. & Erbe, E. F. (1996)Snow crystal imaging using scanning electron microscopy. *Hydrol. Sci. J.* **41**(2), 219–233.

Sverdrup, H. U. (1936)The eddy conductivity of the air over a smooth snow field. *Geofysiske Publikasjoner* **11**(7).

Thorpe, A. D. & Mason, B. J. (1966)The evaporation of ice spheres and ice crystals. *Brit. J. Appl. Phys.* **17**, 541–548.

Wania, F. (1997) Modelling the behaviour of non-polar organic chemicals in an aging snowpack. *Chemosphere* **35**, 2345–2363.

Williams, G. P. (1959) Evaporation from snow covers in Eastern Ontario. *National Research Council of Canada, Division of Building Research, Res. Pap. no. 73.*